Nonlinear Ripple Dynamics on Amorphous Surfaces Patterned by Ion Beam Sputtering

Javier Muñoz-García,[1] Mario Castro,[2] and Rodolfo Cuerno[1]

[1]*Departamento de Matemáticas and Grupo Interdisciplinar de Sistemas Complejos (GISC),*
Universidad Carlos III de Madrid, Avenida de la Universidad 30, E-28911 Leganés, Spain
[2]*GISC and Grupo de Dinámica No Lineal (DNL), Escuela Técnica Superior de Ingeniería (ICAI),*
Universidad Pontificia Comillas, E-28015 Madrid, Spain

Erosion by ion-beam sputtering (IBS) of amorphous targets at off-normal incidence frequently produces a (nanometric) rippled surface pattern, strongly resembling macroscopic ripples on aeolian sand dunes. A suitable generalization of continuum descriptions of the latter allows us to describe theoretically for the first time the main nonlinear features of ripple dynamics by IBS, namely, wavelength coarsening and nonuniform translation velocity, that agree with similar results in experiments and discrete models. These properties are seen to be the anisotropic counterparts of in-plane ordering and (interrupted) pattern coarsening in IBS experiments on rotating substrates and at normal incidence.

Ever since their earliest observation [1], the production of ripples on the surfaces of amorphous targets subject to ion-beam sputtering (IBS) at intermediate energies has been fascinating due to the similarities with macroscopic ripples, like those produced underwater [2], or on the surface of aeolian sand dunes [3]. Beyond the morphological resemblance, IBS ripples share many other properties with, e.g., aeolian ripples, such as wavelength coarsening and pattern translation with time [4,5]. Remarkably, while typical wavelengths of the latter are above 1 cm, the periodicity of IBS ripples is in the 100 nm range [6], these patterns having gained increased interest recently for applications in nanotechnology, ranging from optoelectronic to catalytic [7]. IBS ripples are produced on a wide class of substrates, from amorphous or amorphizable (silica, Si, GaAs, InP) to metallic targets (Cu, Au, Ag) [6]. In view, moreover, of their implied loss of in-plane symmetry, IBS ripples provide interesting instances of systems hosting a competition between pattern forming and disordering mechanisms [8].

A successful description of the main features of IBS ripples was provided by Bradley and Harper (BH) [9], based on Sigmund's linear cascade approximation of sputtering processes in amorphous or polycrystalline targets [10]. The linear equation derived by BH describes satisfactorily some properties of IBS ripples, such as their alignment with the ion beam as a function of the incidence angle to target normal θ [wave vector parallel (perpendicular) to the projection of the ion beam for $\theta < \theta_c$ ($\theta > \theta_c$), for some threshold θ_c]. Other features, such as ripple stabilization or wavelength dependence with ion energy or flux, required nonlinear extensions of BH's approach [11,12], leading to an anisotropic generalization of the well-known Kuramoto-Sivashinsky (KS) equation [8,11]. However, a notable limitation of the anisotropic KS (AKS) equation is its inability to predict ripples that coarsen with time, contradicting observations in many experiments and/or discrete models of IBS (see [5,13] and references therein).

In this Letter, we introduce a ''hydrodynamic'' model [3,14,15] for IBS ripple production at off-normal incidence. Time scale separation between microscopic processes (collision cascades, surface diffusion) and pattern evolution allows us to derive an improved equation for the surface height. The new nonlinear terms appearing allow for ripple coarsening and pattern translation with nonuniform velocity, as seen in experiments and discrete models. Our theory has both the AKS equation [11] and the hydrodynamic theory [15] proposed for normal incidence conditions [16] as particular limits, and enables analysis of the important case of rotating substrates [17]. In addition, our model may be important also to the context of ripples on aeolian sand dunes, where the standard 1D approximation requires validation, fully anisotropic 2D models being scarce [3], as incidentally occurs in many other contexts within pattern formation [18].

During IBS of amorphous or semiconductor substrates, in which the ions amorphize the subsurface layer, incident ions lose their energy through random collision cascades in the bulk [10]. Near-surface atoms receiving enough energy and momentum to break their bonds are in principle sputtered away, although they may join the current of surface adatoms that are available to other relaxation mechanisms, such as surface diffusion, before incorporating back to the solid bulk. Within the so-called hydrodynamic approach to aeolian sand dunes [3] and ion-sputtered surfaces [14,15], we consider two coupled fields, namely, the thickness of the mobile surface adatoms layer, $R(\mathbf{x}, t)$, (related with the density of mobile adatoms through the atomic volume) and the height of the bombarded surface above a reference plane, $h(\mathbf{x}, t)$. Their time evolution is provided by

$$\partial_t R = (1 - \phi)\Gamma_{\mathrm{ex}} - \Gamma_{\mathrm{ad}} + D\nabla^2 R, \qquad (1)$$

$$\partial_t h = -\Gamma_{\mathrm{ex}} + \Gamma_{\mathrm{ad}}, \qquad (2)$$

where Γ_{ex} and Γ_{ad} are, respectively, rates of atom excavation from and addition to the immobile bulk, $(1 - \phi) = \bar{\phi}$ measures the fraction of eroded atoms that become mobile,

and the third term in Eq. (1) describes motion of mobile atoms along the surface as due to isotropic thermal diffusion (D being a constant for amorphous materials). Even if all eroded atoms are sputtered away ($\phi = 1$), we assume a nonzero average fraction of mobile atoms, R_{eq}.

Under the assumption that nucleation events are more likely in surface protrusions, in analogy to the Gibbs-Thompson relation we have

$$\Gamma_{\mathrm{ad}} = \gamma_0[R(1 + \gamma_{2x}\partial_x^2 h + \gamma_{2y}\partial_y^2 h) - R_{\mathrm{eq}}], \quad (3)$$

where γ_0 is the mean nucleation rate for a flat surface (on the xy plane) and γ_{2x}, $\gamma_{2y} \geq 0$ describe variation of the nucleation rate with surface curvatures. Note that, in (3), the full thickness of the mobile adatoms layer is affected by the shape of the surface.

The rate at which material is sputtered from the bulk depends on the angle of incidence, ion and substrate species, ion flux, energy, and many other experimental parameters. If the beam direction is in the xz plane, we have, following [11,15]

$$\Gamma_{\mathrm{ex}} = \alpha_0[1 + \alpha_{1x}\partial_x h + \alpha_{2x}\partial_x^2 h + \alpha_{2y}\partial_y^2 h + \alpha_{3x}(\partial_x h)^2$$
$$+ \alpha_{3y}(\partial_y h)^2 - (\partial_x h)(\alpha_{4x}\partial_x^2 h + \alpha_{4y}\partial_y^2 h)], \quad (4)$$

where parameters reflect the dependence of Γ_{ex} on the *local* shape of the surface [19], as described by more microscopic derivations such as BH or generalizations thereof [11,20]. Analogous, but not equal, geometrical couplings to the driving occur in aeolian sand dunes [3], or in *growth* onto amorphous substrates [21]. Note the loss of reflection symmetry in the x direction, but not in the y direction. For a planar surface, atoms are sputtered from the bulk in a typical time of order α_0^{-1}.

The main difference between former models [9,11,12] and our present model, Eqs. (1)–(4), is that, in the latter, eroded material is allowed to redeposit locally, and there is an implicit viscous flow [22] in the amorphized layer through the evolution of R. These *additional mechanisms* are seen below to induce richer pattern dynamics than in [9,11,12].

The linearized Eqs. (1)–(4) have solutions $R^l = \hat{R}^l e^{i\mathbf{k}\cdot\mathbf{x}+\omega_\mathbf{k} t}$, $h^l = \hat{h}^l e^{i\mathbf{k}\cdot\mathbf{x}+\omega_\mathbf{k} t}$, with a dispersion relation, $\omega_\mathbf{k}$, given in the long wavelength limit by [19]

$$\mathrm{Re}(\omega_\mathbf{k}) = \epsilon\phi\gamma_0(\alpha_{2x}k_x^2 + \alpha_{2y}k_y^2) - \epsilon^2\phi\bar{\phi}\gamma_0\alpha_{1x}^2 k_x^2$$
$$- R_{\mathrm{eq}}D(k_x^2 + k_y^2)(\gamma_{2x}k_x^2 + \gamma_{2y}k_y^2) + \mathcal{O}(\epsilon k^4), \quad (5)$$

$$\mathrm{Im}(\omega_\mathbf{k}) = -\epsilon\phi\gamma_0\alpha_{1x}k_x + \mathcal{O}(k^3), \quad (6)$$

where $\epsilon \equiv \alpha_0/\gamma_0$ is a dimensionless parameter; the erosion rate being much smaller than the nucleation rate, $\epsilon \ll 1$ for typical experiments. Equation (6) is a simple consequence of the asymmetry in the x direction, induced by the incoming flux.

The surface morphology is dominated by the periodic pattern with wave vector $\mathbf{k}^{\mathrm{max}}$ making Eq. (5) a positive maximum. It can be shown [19] that $\mathbf{k}^{\mathrm{max}}$ is oriented along the $\hat{\mathbf{x}}$ or $\hat{\mathbf{y}}$ directions, as observed experimentally [6]. Close to the instability threshold, before nonlinear terms are no longer negligible, one has $k_{x,y}^{\mathrm{max}} \sim \epsilon^{1/2}$. Substituting this into Eqs. (5) and (6) provides us with estimations of the typical time and length scales of the pattern, that we employ to rescale $X = \epsilon^{1/2}x$, $Y = \epsilon^{1/2}y$, $T_2 = \epsilon^2 t$, and $T_1 = \epsilon^{3/2}t$, and perform a multiple scale expansion of Eqs. (1) and (2), in which R can be adiabatically eliminated. To lowest nonlinear order, we get [19,23]

$$\partial_t h = \gamma\partial_x h + \sum_{i=x,y}\{-\nu_i\partial_i^2 h + \lambda_i^{(1)}(\partial_i h)^2$$
$$+ \Omega_i\partial_i^2\partial_x h + \xi_i(\partial_x h)(\partial_i^2 h)\}$$
$$+ \sum_{i,j=x,y}\{-\mathcal{K}_{ij}\partial_i^2\partial_j^2 h + \lambda_{ij}^{(2)}\partial_i^2(\partial_j h)^2\};$$

$$\gamma = -\epsilon\phi\gamma_0\alpha_{1x}, \qquad \nu_x = \epsilon\phi\gamma_0\alpha_{2x} - \epsilon^2\bar{\phi}\phi\gamma_0\alpha_{1x}^2,$$
$$\nu_y = \epsilon\phi\gamma_0\alpha_{2y}, \qquad \lambda_i^{(1)} = -\epsilon\phi\gamma_0\alpha_{3i},$$
$$\Omega_i = \epsilon(\bar{\phi}D - \phi R_{eq}\gamma_0\gamma_{2i})\alpha_{1x}, \qquad \xi_i = \epsilon\phi\gamma_0\alpha_{4i},$$
$$\mathcal{K}_{ij} = DR_{\mathrm{eq}}\gamma_{2i} + \epsilon[D\bar{\phi}(\gamma_{2i} - \alpha_{2j}) + \phi\gamma_0 R_{\mathrm{eq}}\gamma_{2i}\alpha_{2j}],$$
$$\lambda_{ij}^{(2)} = \epsilon[\bar{\phi}D - \phi R_{\mathrm{eq}}\gamma_0\gamma_{2i}]\alpha_{3j}. \quad (7)$$

Equation (7) generalizes the AKS-type equations obtained [9,11,12] within BH approach to IBS. While sharing the same reflection properties in the x and y directions and most of the terms on the rhs, both equations differ crucially by the presence here of the $\lambda_{ij}^{(2)}$ nonlinearities. Moreover, in the absence of redeposition ($\phi = 1$), $\lambda_i^{(1)}$ and $\lambda_{ij}^{(2)}$ have the same signs, making Eq. (7) nonlinearly unstable, as in the BH case [15,24,25]. Note, the linear dispersion relation of (7) matches Eqs. (5) and (6) above. Under normal incidence, parameters are isotropic and $\alpha_{1x} = \alpha_{4x} = \alpha_{4y} = 0$, Eq. (7) reducing to that obtained in [15,24], and in [21]. As a final remark, let us quote the form of Eq. (7) for *sample rotation* around the z axis during bombardment (see, e.g., [17,26]). Dynamics of h are given by a different isotropic limit of Eq. (7), namely,

$$\partial_t h = -\nu_r\nabla^2 h - \mathcal{K}_r\nabla^4 h + \lambda_r^{(1)}(\nabla h)^2$$
$$+ \lambda_r^{(2)}\nabla^2(\nabla h)^2 + \lambda_r^{(3)}\nabla\cdot[(\nabla^2 h)\nabla h];$$

$$\nu_r = (\nu_x + \nu_y)/2, \qquad \lambda_r^{(1)} = (\lambda_x^{(1)} + \lambda_y^{(1)})/2,$$
$$\lambda_r^{(2)} = \frac{1}{4}\sum_{i,j=x,y}\lambda_{i,j}^{(2)}, \qquad \lambda_r^{(3)} = \frac{1}{2}\sum_{i,j=x,y}\lambda_{i,j}^{(2)}\delta_{i,j} - \lambda_r^{(2)}, \quad (8)$$
$$\mathcal{K}_r = (3\mathcal{K}_{x,x} + 3\mathcal{K}_{y,y} + \mathcal{K}_{x,y} + \mathcal{K}_{y,x})/8,$$

with parameters (subscript "r" denotes "rotating").

To the best of our knowledge, Eq. (7) is new, and indeed has a rich parameter space. Numerical integration (not shown) within linear regime retrieves all features of the ripple structure as predicted by the BH theory, i.e., dependence of the ripple wavelength with linear terms, and ripple orientation as a function of θ. Entering the nonlinear regime, and as occurs in the AKS equation and its generalizations [11,12], nonlinearities $\lambda_i^{(1)}$ lead to saturation of the pattern with constant wavelength and amplitude. In absence of these terms, the ripple wavelength grows indefinitely as $l(t) \sim t^n$ with $n = 1/2$ [27,28] until a single ripple remains in a finite simulation domain. As an anisotropic generalization of the ordering process observed for normal incidence [15,16], pattern coarsening requires the presence of $\lambda_{i,j}^{(2)}$, whose magnitude and mathematically correct sign [25] are due to describing redeposition by means of the additional field R. When the values of these coefficients increase relative to $\lambda_i^{(1)}$, coarsening stops later, and the amplitude and wavelength of the pattern also increase. The coarsening exponent n will take an *effective* value that will be larger the later coarsening stops, and may depend on simulation parameter values. For instance, we show in Fig. 1 snapshots of a numerical integration of Eq. (7) for relatively large $\lambda_{i,j}^{(2)}$. The apparent coarsening is quantified in the plot of $l(t)$ shown in Fig. 2(a), compat-

ible (after transient effects analogous to those in [27]) with $n = 0.19$. Note the saturation of ripple wavelength at long times, together with saturation in amplitude, as shown in the plot of the surface roughness (rms width) $W(t)$ in Fig. 2(b). These results are similar to those obtained experimentally for IBS of Si in [4]. For a different experiment on Si, precise measurements of the coarsening exponent [5] yield $n = 0.50(4)$, no saturation having been observed in this system, as we would expect. Here, the dispersion velocity of the pattern was also measured, finding that it decays with ripple wavelength or, equivalently, with time. We have also observed the same trend in the dispersion velocity of the ripples shown in Fig. 1. Experiments also exist, e.g., for IBS of Si, in which ripple coarsening is absent or residual [29], that would correspond to smaller $\lambda_{i,j}^{(2)}$ values in (7), see, e.g., an example in Fig. 3, where $\ell(t) \sim \log t$, approximately. Ripple coarsening has been also observed in a Monte Carlo model of IBS [13], in which rules implement Sigmund's theory. To our purpose, the main conclusion of this study is the correlation between an increasing $l(t)$ and nonuniform dispersion velocity, and on the parameter-dependent values of the coarsening exponent. Let us note that, on the experimental side, values of n show a large scatter in the literature (see references in [6,13]). Additional nonlinear effects can be described by Eq. (7). A *first* one is production of grooves (as opposed to ripples), due to the loss of up-down symmetry induced by quadratic nonlinearities. Indeed, by changing the sign of $\lambda_i^{(1)}$, grooves replace ripples, see Fig. 1(d); this calls for systematic experimental exploration. A *second* effect is
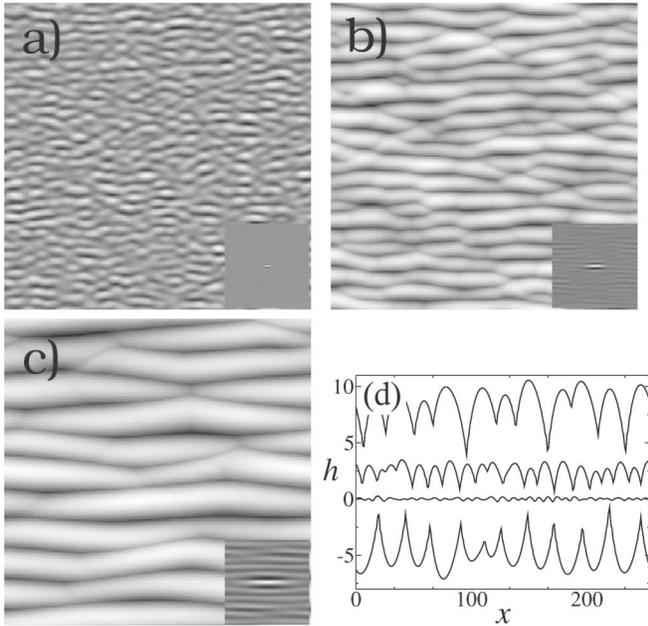

FIG. 1.   Numerical integration of Eq. (7) using $\nu_x = 1$, $\nu_y = 0.1$, $\Omega_x = 1$, $\Omega_y = 0.5$, $\xi_i = 0.1$, $\lambda_x^{(1)} = 0.1$, $\lambda_y^{(1)} = 5$, $\lambda_{i,j}^{(2)} = -5$, $\mathcal{K}_{i,j} = 1$. Top views for $t = 10, 106, 953$ (a), (b), and (c), respectively. Insets are height autocorrelations. All units are arbitrary. (d): Top to bottom, side cuts of (c), (b), (a), and grooves obtained for sign changed $\lambda_{x,y}^{(1)}$ and $\lambda_{i,j}^{(2)}$. Curves have an artificial offset.
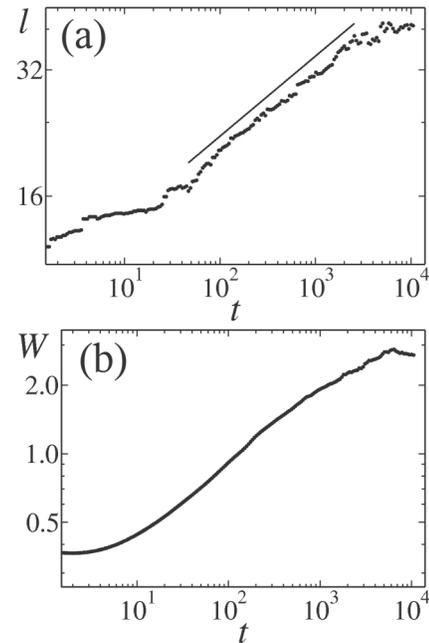

FIG. 2.   Ripple wavelength $l(t)$ and surface roughness $W(t)$ for parameters as in Fig. 1. The straight line represents $l \sim t^{0.19}$. All units are arbitrary.
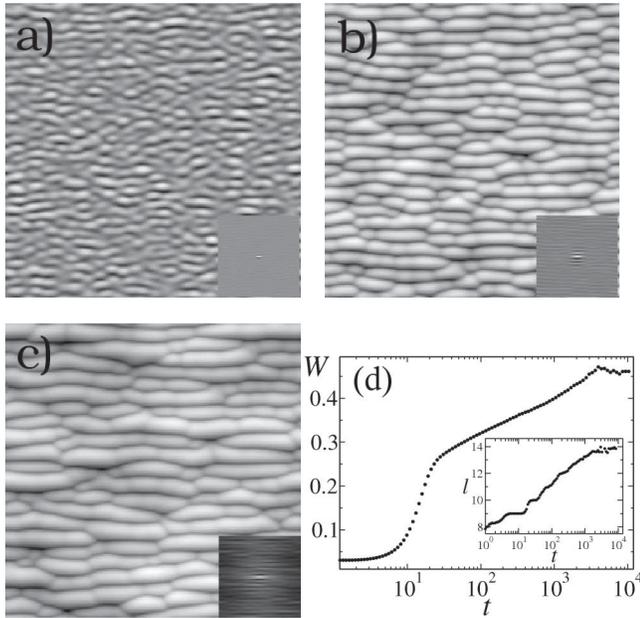
FIG. 3.　Numerical integration of Eq. (7) for parameters as in Fig. 1, except for $\lambda_x^{(1)} = 1$. Top views for $t = 10, 106, 953$ (a), (b), and (c), respectively. (d): Surface roughness $W(t)$ for the same simulation. Inset: $l(t)$ for the same system, showing marginal coarsening. All units are arbitrary.

related with cancellation modes (CM), known in the AKS equation [12,30] and other models of IBS [14,15,24]. These are linearly unstable modes for which nonlinearities cancel one another exactly. While for equations like the one considered in [15,21] CM affects well posedness, anisotropic systems [12,30] may remain better defined in the presence of CM. In our case, if reflection symmetry breaking terms are neglected in Eq. (7) and BH parameters are used, the same CM occur as in the AKS equation. Additional CM ensue between the $\lambda_i^{(1)}$ and $\lambda_{i,j}^{(2)}$ terms for appropriate relative signs [21,25]. We have verified numerically that the *full* Eq. (7) breaks down for the latter CM, but can support AKS-type CM. That these solutions are physically realizable or are artifacts of the small slope approximation made, remains to be assessed. Useful information on this issue might come from field experiments in aeolian sand dunes.

In closing, we mention IBS of metals as an immediate experimental domain to which the above results may be relevant [6], albeit differing in the degree of universality. There, however, the correct extension of BH theory is not yet clear, nor is its importance relative to anisotropic surface diffusion. We have taken preliminary steps in this context [20], and expect to make progress in this direction soon.

[1]　M. Navez, C. Sella, and D. Chaperot, C. R. Acad. Sci. Paris **254**, 240 (1962).
[2]　A. Stegner and J. E. Wesfreid, Phys. Rev. E **60**, R3487 (1999).
[3]　O. Terzidis, P. Claudin, and J.-P. Bouchaud, Eur. Phys. J. B **5**, 245 (1998); A. Valance and F. Rioual, Eur. Phys. J. B **10**, 543 (1999); Z. Csahók *et al.*, Eur. Phys. J. E **3**, 71 (2000).
[4]　G. Carter and V. Vishnyakov, Phys. Rev. B **54**, 17 647 (1996).
[5]　S. Habenicht *et al.*, Phys. Rev. B **65**, 115327 (2002).
[6]　U. Valbusa, C. Boragno, and F. Buatier de Mongeot, J. Phys. Condens. Matter **14**, 8153 (2002).
[7]　M. V. R. Murty, Surf. Sci. **500**, 523 (2002); O. Azzaroni *et al.*, Adv. Mater. **16**, 405 (2004).
[8]　M. C. Cross and P. C. Hohenberg, Rev. Mod. Phys. **65**, 851 (1993).
[9]　R. M. Bradley and J. M. Harper, J. Vac. Sci. Technol. A **6**, 2390 (1988).
[10]　P. Sigmund, Phys. Rev. **184**, 383 (1969); J. Mater. Sci. **8**, 1545 (1973).
[11]　R. Cuerno and A.-L. Barabási, Phys. Rev. Lett. **74**, 4746 (1995); M. Makeev, R. Cuerno, and A.-L. Barábasi, Nucl. Instrum. Methods Phys. Res., Sect. B **197**, 185 (2002).
[12]　S. Park *et al.*, Phys. Rev. Lett. **83**, 3486 (1999).
[13]　E. Yewande, A. K. Hartmann, and R. Kree, Phys. Rev. B **71**, 195405 (2005).
[14]　T. Aste and U. Valbusa, Physica A (Amsterdam) **332**, 548 (2004); New J. Phys. **7**, 122 (2005).
[15]　M. Castro *et al.*, Phys. Rev. Lett. **94**, 016102 (2005).
[16]　S. Facsko *et al.*, Science **285**, 1551 (1999); R. Gago *et al.*, Appl. Phys. Lett. **78**, 3316 (2001).
[17]　F. Frost, A. Schindler, and F. Bigl, Phys. Rev. Lett. **85**, 4116 (2000).
[18]　D. E. Bar and A. A. Nepomnyashchy, Physica D (Amsterdam) **132**, 411 (1999).
[19]　J. Muñoz-García, M. Castro, and R. Cuerno (to be published).
[20]　M. Feix *et al.*, Phys. Rev. B **71**, 125407 (2005).
[21]　M. Raible *et al.*, Europhys. Lett. **50**, 61 (2000); M. Raible, S. J. Linz, and P. Hänggi, Phys. Rev. E **64**, 031506 (2001).
[22]　C. C. Umbach *et al.*, Phys. Rev. Lett. **87**, 246104 (2001).
[23]　In principle, Eq. (7) does not cover the conserved $\phi = 0$ limit (irrelevant to IBS), where a different expansion must be used, as seen from Eqs. (5) and (6).
[24]　T. C. Kim *et al.*, Phys. Rev. Lett. **92**, 246104 (2004).
[25]　M. Castro and R. Cuerno, Phys. Rev. Lett. **94**, 139601 (2005); T. C. Kim *et al.*, *ibid.* **94**, 139602 (2005).
[26]　R. M. Bradley, Phys. Rev. E **54**, 6149 (1996).
[27]　M. Raible, S. J. Linz, and P. Hänggi, Phys. Rev. E **62**, 1691 (2000).
[28]　This is in absence of advective terms. Otherwise, even larger exponent values are possible [19].
[29]　J. Erlebacher *et al.*, Phys. Rev. Lett. **82**, 2330 (1999).
[30]　M. Rost and J. Krug, Phys. Rev. Lett. **75**, 3894 (1995).